CONDENSED MATTER

Anatomy of the Band Structure of the Newest Apparent Near-Ambient Superconductor $LuH_{3-x}N_x$

N. S. Pavlov[a,b,*], I. R. Shein[c], K. S. Pervakov[b], V. M. Pudalov[b], and I. A. Nekrasov[a,b]

[a] *Institute of Electrophysics, Ural Branch, Russian Academy of Sciences, Yekaterinburg, 620016 Russia*
[b] *Lebedev Physical Institute, Russian Academy of Sciences, Moscow, 119991 Russia*
[c] *Institute of Solid State Chemistry, Ural Branch, Russian Academy of Sciences, Yekaterinburg, 620108 Russia*
*e-mail: pavlovns@lebedev.ru

Recently it was claimed that nitrogen-doped lutetium hydride exhibited a near-ambient superconducting transition with a temperature of 294 K at a pressure of only 10 kbar, this pressure being several orders of magnitude lower than previously demonstrated for hydrides under pressure. In this paper, we investigate within DFT + U the electronic structure of both parent lutetium hydride LuH_3 and nitrogen doped lutetium hydride $LuH_{2.75}N_{0.25}$. We calculated corresponding bands, density of states and Fermi surfaces with and without spin-orbit coupling (SOC). It is shown that in the stoichiometric system the Lu-5d states cross the Fermi level while the H-1s states make almost no contribution at the Fermi level. However, with nitrogen doping, the N-2p states enter the Fermi level in large quantities and bring together a significant contribution from the H-1s states. The presence of N-2p and H-1s states at the Fermi level in a doped compound can facilitate the emergence of superconductivity. Surprisingly, SOC splits quite significantly (0.1−0.25 eV) nitrogen bands in $LuH_{2.75}N_{0.25}$ just below the Fermi level. For instance, nitrogen doping almost doubles the value of DOS at the Fermi level. Simple BCS analysis shows that the nitrogen doping of LuH_3 can provide T_c more than 100 K and even increase it with further hole doping.

INTRODUCTION

The discovery of high temperature superconductivity under high pressure around 100−250 GPa with T_c about 203 K in a hydrogen-containing H_3S system [1] gave rise to a flow of experimental and theoretical works (see reviews [2−7]). The subsequent discovery of near-room temperature superconductivity in hydrides brings us back to the classical electron-phonon superconducting pairing, very likely consistent within the Bardeen−Cooper−Schriefer (BCS) theory. Remarkably, there appeared many different classes of hydrides under pressure and the band structure calculations (density functional theory—DFT) have shown the ability to predict crystal structures and T_c values for many of those hydrides [7−12].

The stunning experimental discovery of the near room temperature superconductors in the so-called hydrides under high-pressure indeed is the hottest topic in modern physics. For potential practical applications of this class of superconductors it is crucial to lower the value of the external pressure at which superconductivity occurs. Here we address the issue of superconductivity in the recently discovered nitrogen doped superconducting rare-earth hydrides. Recent report on apparent superconductivity in the nitrogen-doped lutetium hydride LuH_xN_y with $T_c = 294$ K at 10 kbar [13], has sparked intensive theoretical and experimental research.

Three months later, resistivity measurements on the same samples from [13] were repeated by another scientific group and showed the superconductivity with $T_c = 240$ K at 8.5 kbar [14] and above. However, in [14] some samples did not superconduct due to the way of preparation as marked by the authors. There are many theoretical works on the crystal structure of LuH_xN_y, which is most stable at given experimental conditions [15−20]. Also these works report the calculated phonon spectra and provide estimation of the possible BCS-type superconductivity. Strictly speaking, none of these works demonstrate the emergence of BCS-type superconductivity with $T_c = 294$ K at 10 kbar. In addition, it has also been suggested that there may exist a more stable LuH_2 phase of the CaF_2-type ($Fm\overline{3}m$) with a very low $T_c = 0.026$ K [21].

In the paper [22], it was shown that taking into account temperature and quantum anharmonic lattice effects in the phonon calculations for LuH_3 stabilizes

the lattice within the $Fm\overline{3}m$ space group at pressure up to 4.4 GPa and temperature of 150 K. The superconductivity with T_c value in the range of 50–60 K is also obtained in [22]. The non-trivial topology of bands and surface states near the Fermi level of stoichiometric LuH₃ was found in [23]. The optical spectra of LuH_2 ($Fm\overline{3}m$), LuH ($P\overline{4}3m$), LuH ($F\overline{4}3m$) and LuN ($Fm\overline{3}m$) were theoretically investigated in [24]. Based on DFT calculations the reflectivity of LuH_2 ($Fm\overline{3}m$) was found to explain the observed colour change under pressure [25]. Extended theoretical comments on the original paper [13] were presented in [26]. Identification of classes of structures and hydrogen-vacancy ordering schemes for Lu–H–N properties was performed in [27]. Ab initio calculations of the structural, vibrational and optical properties LuH_2 and LuH_3 were reported in [28].

There are also several experimental attempts to reproduce the original results [13] with the same chemical compositions or newly synthesized samples. The resistivity and magnetic properties of Lu, LuH_2 were measured [29] at temperatures from 300 to 2 K. Here, the resistivity of lutetium dihydride was found to be temperature independent. The resistivity measurements for both LuH_2 and LuH_3 showed no evidence of superconductivity [30] in the temperature range of 300–4 K and pressure range of 0.9–3.4 GPa. Also magnetic susceptibility measurements in the pressure range of 0.8–3.3 GPa and temperatures down to 100 K did not show any signatures of superconductivity. The resistivity and specific heat of LuH_2 were measured in [31]. It is shown that percolation of the metallic micro grains through the insulating surfaces produces a sharp drop in resistivity. The resistivity measurements in [32] with LuH_2 under elevated pressures up to ∼7 GPa did not reveal superconductivity down to 1.5 K.

The nitrogen-doped compound $LuH_{2\pm x}N_y$ showed a metallic behavior without superconductivity down to 10 K and pressures from 1 to 6 GPa [33]. Possible structural/electronic phase transition between two non-superconducting phases was observed in $LuH_{2\pm x}N_y$ [34], which is most pronounced in the "pink" phase and might have been erroneously interpreted as a sign of superconducting transition. The resistivity of $LuH_{2\pm x}N_y$ under pressures up to 50.5 GPa exhibited progressively optimized metallic behavior with pressure [35]. The reflectivity of LuH_2 under pressure was investigated in [36] and was found to change significantly in the visible spectrum due the plasmon resonance. In addition, the pressure-induced color change in $LuH_{2\pm x}N_y$ was observed in [37] up to 33 GPa. Raman spectroscopy and X-ray diffraction were used to characterize the crystal structure of LuH_3 at various pressures [38]. Single-crystalline films of LuH_{2+x} were studied in [39] using Raman spectroscopy and electrical transport measurements. In [40]

magnetic susceptibility was measured for the sample Lu–N–H at pressure up to 4.3 GPa and did not show the superconductivity. Besides the original claim made in [13] and recently in [14], in another work [41] superconductivity with $T_c = 71$ K at 218 GPa was found, presumably for the LuH system with the space symmetry group $Fm\overline{3}m$. With lowering pressure to 181 GPa, T_c decreases down to 65 K [41], thus approaching the results previously reported in [42] for LuH_3 ($T_c = 12.4$ K at 122 GPa).

At this moment we are not aware of any detailed study of band structure of the N-doped lutetium hydride $LuH_{3-x}N_x$ ($x = 0.25$), the compound that was presumably synthesized in original work [13], and its relation to that for the parent LuH_3 compound. In this paper we performed DFT + U band structure calculations (including spin-orbit coupling) of both parent lutetium hydride LuH_3 and nitrogen doped lutetium hydride $LuH_{2.75}N_{0.25}$. We calculated the bands with orbital contributions, density of states and Fermi surfaces. Within the framework of the Wannier projection method, a minimal model which gives good description of the bands crossing the Fermi level is found. In particular, our analysis reveals the contribution of nitrogen levels in the density of states at the Fermi level and in the formation of superconducting state. We also provide simple BCS-analysis of T_c for materials under consideration.

COMPUTATIONAL DETAILS

The calculations were performed within the DFT + U approximation in the VASP software package [43]. The generalized gradient approximation (GGA) in the form of the Perdew–Burke–Ernzerhof (PBE) exchange-correlation functional [44] was employed. The strong onsite Coulomb repulsion of Lu-4f electrons was described with the DFT + U scheme with the Dudarev approach [45] ($U = 5.0$ eV).

We consider the parent lutetium hydride LuH_3 and nitrogen doped lutetium hydride $LuH_{2.75}N_{0.25}$ with the spatial symmetry group $Fm\overline{3}m$ and lattice parameter $a = 5.0289$ Å [13] at ambient pressure. We select this parameters corresponding to the ambient condition, because the band structure and density of states are practically the same as those for parameter $a = 5.007$ Å determined experimentally at pressure of 1 GPa [13]. The H atoms are located in positions with tetrahedral (0.25, 0.25, 0.25) and octahedral (0.5, 0, 0) surroundings of Lu atoms (Fig. 1). The Lu atoms are located at the point of origin, at (0, 0, 0). To get $LuH_{2.75}N_{0.25}$ system, only one of the four hydrogen atoms at octahedral surrounding is replaced by the nitrogen atom, since such substitution, as shown in the work [13], leads to a metal. The ion relaxation was done for $LuH_{2.75}N_{0.25}$. In [17] it was found that the
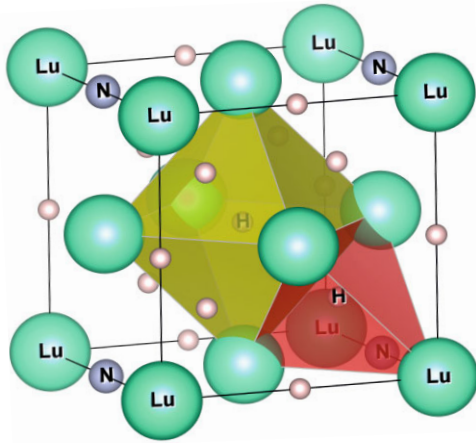
Fig. 1. (Color online) Crystal structure of $LuH_{2.75}N_{0.25}$ with two types of H atom surroundings (yellow—octahedral, red—tetrahedral).
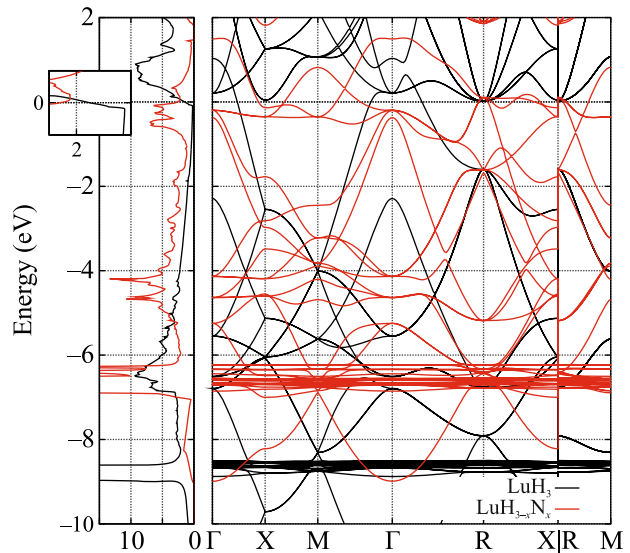

Fig. 2. (Color online) GGA + U (left panel) total densities of states and (right panel) band dispersions of LuH_3 (black lines), $LuH_{2.75}N_{0.25}$ (red lines). The inset on left panel shows the densities of states near the Fermi level [−0.5; 0.5] eV. Note that the DOS curves are shifted relative each other to superpose the Fermi levels at zero energy.

enthalpy of formation of $LuH_{2.75}N_{0.25}$ is negative at 1 GPa, which means that this compound can be formed. The full unit cell was calculated in order to enable comparison of LuH_3 and $LuH_{2.75}N_{0.25}$.

Wannier functions were obtained using the Wannier90 [46] package with projection onto H-1s in octahedral environment and N-2p orbitals.

RESULTS

The comparison of GGA + U total densities of states (left panel) and band dispersions (right panel) between LuH_3 (black lines) and $LuH_{2.75}N_{0.25}$ (red lines) is shown on Fig. 2.

Nitrogen doping leads to formation of a wide peak in the total density of states (DOS) just below the Fermi level (red line on the left panel of Fig. 2), in contrast to the case of stoichiometric LuH_3. The most important is that the total density of states at the Fermi level increases almost by a factor of two in $LuH_{2.75}N_{0.25}$, from 1.5 to 2.6 states/eV/u.c. (left panel of Fig. 2). Later we will use this fact to estimate the possible superconducting T_c value.

For both compounds we have well pronounced three dimensional bands. The substitution of hydrogen atom by nitrogen one gives four additional holes per unit cell which leads to the ~1.8 eV lowering of the Fermi level in $LuH_{2.75}N_{0.25}$ as compared to LuH_3. Although the bands can not be superposed by their simple shift, some features are quite similar for both systems.

In the case of $LuH_{2.75}N_{0.25}$ there are several bands which cross the Fermi level at each high-symmetry direction, while for LuH_3 only couple of bands near the Γ-point cross the Fermi level. For $LuH_{2.75}N_{0.25}$ at the Fermi level there are pronounced flat band regions

in the vicinity of R and X points, which are missing for LuH_3. These local flat bands are favourable to superconducting pairing. Near R-point both compounds have bands nearly touching the Fermi level.

Due to the local Coulomb interaction, the Lu-4f states are located far away from the Fermi level: near −9 eV in LuH_3 and near −7 eV in $LuH_{2.75}N_{0.25}$ (Fig. 2). In addition, we check several values of U which affect only the position of Lu-4f bands but not the states near the Fermi level.

Surprisingly, in $LuH_{2.75}N_{0.25}$ the account of spin-orbit (SO) coupling splits quite significantly (0.1–0.25 eV) nitrogen bands just below the Fermi level in Γ–X and Γ–R directions (see Fig. 3, blue lines) in contrast to GGA + U bands (red lines). The total value of DOS at the Fermi level in case of GGA + U + SO is practically the same as for the GGA + U case. The Lu-4f bands are also split by spin-orbit coupling, they are located deep under the Fermi level. Since the bands splitting due to spin-orbit coupling does not touch bands crossing the Fermi level, the Fermi surface will not be affected by the spin-orbit coupling.

Let us consider contributions of different orbitals for LuH_3 (a)−(c) and $LuH_{2.75}N_{0.25}$ (d)−(g) in Fig. 4.

In case of LuH_3, the main contribution to the bands above the Fermi level comes from Lu-5d states (Fig. 4c). The H-1s states of hydrogen atoms in octahedral surrounding manifest themselves around 1 eV and below −1.6 eV (Fig. 4a). On the other hand, the H-1s states of hydrogen atoms in tetrahedral sur-
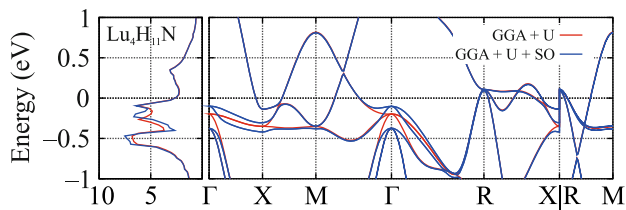
Fig. 3. (Color online) GGA + U (left panel) total densities of states and (right panel) band dispersions of $LuH_{2.75}N_{0.25}$ without (red lines) and with spin−orbit coupling (blue lines). Zero energy is the Fermi level.

rounding lay predominantly below −5 eV (Fig. 4b). In contrast to LuH_3, in case of $LuH_{2.75}N_{0.25}$ the H-1s, Lu-5d and N-2p states contribute to the bands and

density of states at the Fermi level. Since in $LuH_{2.75}N_{0.25}$ there are insufficient electrons to occupy the N-2p states, they are only partially filled. Thus, N-2p bands are located around the Fermi level (Fig. 4g). The N-2p_z states cross the Fermi level, whereas the N-2p_x states lay just below it. The N-2p_y states are fully occupied and are located around −1.5 eV. The H-1s states of hydrogen atoms in octahedral and tetrahedral surroundings lay near the Fermi level (Figs. 4d, 4e). Nevertheless, the main contribution of H-1s states of hydrogen atoms in tetrahedral surrounding is below −3 eV. At the same time, the main contribution of Lu-5d states in $LuH_{2.75}N_{0.25}$ is visible above 1.8 eV (Fig. 4f).
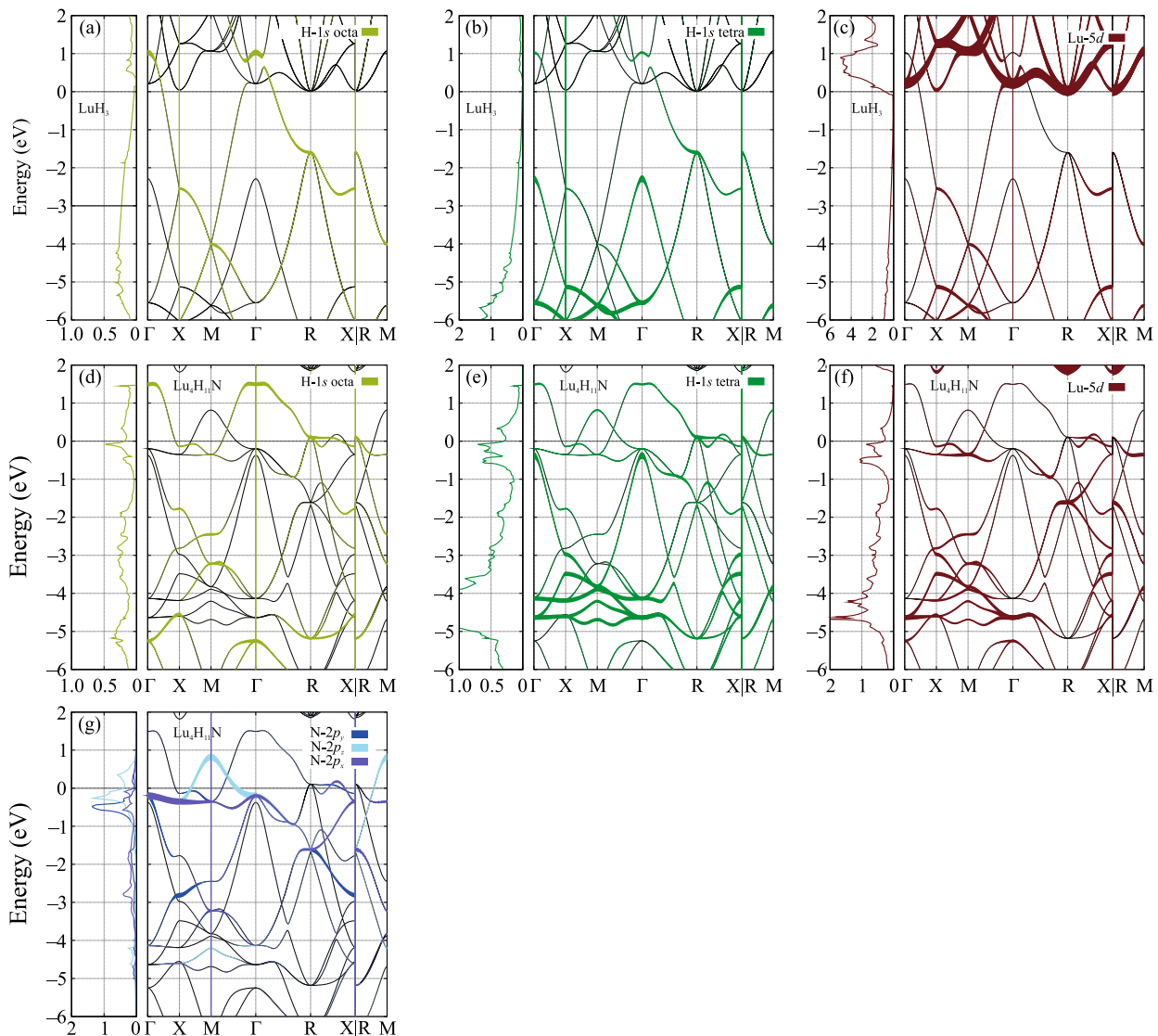

Fig. 4. (Color online) Orbital projected band structure (GGA + U), where the linewidth shows contribution of corresponding orbital: Panels (a), (d) H-1s in octahedral and (b), (e) tetrahedral surrounding, (c), (f) Lu-5d for LuH_3 (upper row) and also (g) N-2p for $LuH_{2.75}N_{0.25}$ (with integer chemical indexes $Lu_4H_{11}N$) (lower row). Zero energy is the Fermi level.
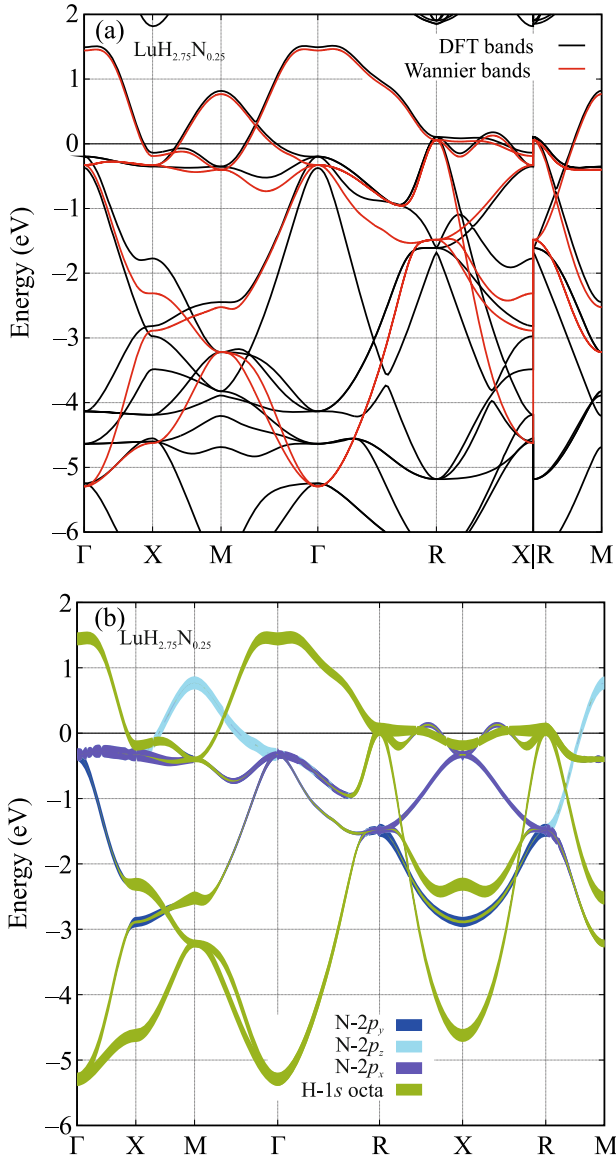
Fig. 5. (Color online) Comparison of original GGA + U bands (black) and projected on Wannier function bands (red lines) (panel (a)). The bands projected on Wannier function with linewidth showing contributions of H-1s octahedral and N-2p states (panel (b)). Zero energy is the Fermi level.

Fig. 6. (Color online) GGA + U calculated Fermi surfaces: (a) LuH_3; (b) $LuH_{2.75}N_{0.25}$.

As a result, the appearance of light element H and N bands with many flat parts on the Fermi level for $LuH_{2.75}N_{0.25}$ compound can lead to a more favorable conditions for superconductivity than in case of the parent LuH_3 system.

In order to define the minimal orbital basis set for $LuH_{2.75}N_{0.25}$, needed to reproduce electronic bands near the Fermi level, we performed projection onto Wannier functions. Comparison of GGA + U bands and bands obtained after Wannier function projection is given on Fig. 5a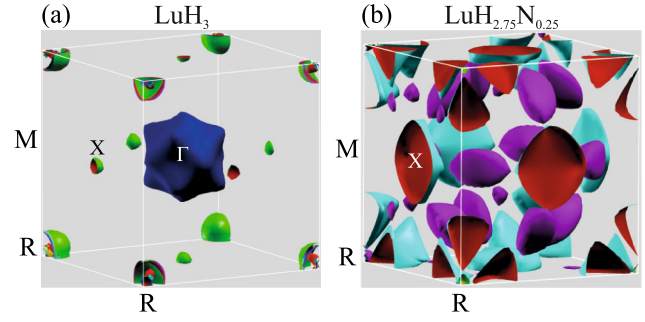. It is determined that to get a good agreement between those bands one needs to include the H-1s state of three H atoms in octahedral surrounding and the N-2p states of the N atom. The bands built on the Wannier functions coincide well enough near the Fermi level with the original GGA + U bands (Fig. 5a), that indicates sufficient reliability of the projecting performed. The orbital character of the bands built on the projected Wannier functions is presented in Fig. 5b. The Projected to Wannier functions Hamiltonian are available online [47].

The Fermi surfaces for LuH_3 (panel (a)) and $LuH_{2.75}N_{0.25}$ (panel (b)) are presented in Fig. 6. A rather large three dimensional Fermi surface sheet of LuH_3 is located around Γ-point. In the corners and face centers of the Brillouin zone there are some small spherical Fermi surface sheets.

For the nitrogen doping case, $LuH_{2.75}N_{0.25}$, the Fermi surface has a more complex structure with many well developed sheets and a pronounced k-dependence.

The most important parameter of superconducting materials is its critical superconducting temperature T_c. To get its simplest rough theoretical estimate, we use the well known BCS equation $T_c = 1.14\omega_D\exp(-1/\lambda)$ with Debye frequency ω_D and dimensionless pairing interaction constant $\lambda = gN(E_F)/2$ (where g is the pairing constant in units of energy, $N(E_F)$ is the value of total DOS at the Fermi level). To find values of ω_D and g we use the data already available in [22].

Correspondingly, we take $T_c^{LuH3} = 62$ K as in [22] obtained with anisotropic Migdal−Eliashberg formalism. The value of $\omega_D = 19.3$ meV $= 220$ K was taken as maximal acoustic phonon energy. Once we know those values we can exclude g from BCS equation and then estimate T_c^{LuHN} value for nitrogen doped material, assuming that ω_D and g do not change significantly:

$$T_c^{LuHN} = 1.14\omega_D(T_c^{LuH_3}/1.14\omega_D)^{N^{LuH_3}(E_F)/N^{LuHN}(E_F)}, \quad (1)$$

where $N^{\mathrm{LuH_3}}(E_\mathrm{F})$ is the total DOS value at the Fermi level for $\mathrm{LuH_3}$, $N^{\mathrm{LuHN}}(E_\mathrm{F})$ is the same but for $\mathrm{LuH_{2.75}N_{0.25}}$. Using Eq. (1) we obtained the value of $T_\mathrm{c} \sim 111$ K for nitrogen doped lutetium hydride $\mathrm{LuH_{2.75}N_{0.25}}$.

Therefore, it can be concluded that nitrogen doping can really increase the T_c value. In the case of further hole doping the density of states at the Fermi level will become higher (Fig. 2). For example, the total density of states has a peak of 6.3 states/eV/u.c. at -0.08 eV. With this value of the total density of states, T_c will be 180 K according to Eq. (1). It corresponds to additional 0.34 holes per unit cell with chemical composition $\mathrm{Lu_4H_{10.92}N_{1.08}}$. Thus, it is theoretically possible to obtain a relatively high T_c value in the $\mathrm{LuH_xN_y}$ compound. Concerning the issue of larger nitrogen doping there appears a problem of lattice stability discussed in the introduction.

CONCLUSION

The comprehensive investigation of the electronic structure of the parent lutetium hydride $\mathrm{LuH_3}$ and nitrogen doped lutetium hydride $\mathrm{LuH_{2.75}N_{0.25}}$ are performed within the DFT + U method including spin-orbit coupling. The band structure, density of states, and Fermi surfaces were obtained and discussed. Surprisingly, in $\mathrm{LuH_{2.75}N_{0.25}}$ the account of spin-orbit coupling splits quite significantly ($0.1-0.25$ eV) nitrogen bands just below the Fermi level in $\Gamma-\mathrm{X}$ and $\Gamma-\mathrm{R}$ directions in contrast to GGA + U bands, while the total value of DOS at the Fermi level stays the same in both cases. The Lu-$5d$ states cross the Fermi level in the stoichiometric system $\mathrm{LuH_3}$, while N-$2p$ states enter the Fermi level in large quantities after nitrogen doping, bringing a significant contribution of the H-$1s$ states. It is shown within projection onto Wannier functions, that taking into account only the N-$2p$ and H-$1s$ states of hydrogen atom in the octahedral surrounding is sufficient for a good description of the bands crossing the Fermi level in case of $\mathrm{LuH_{2.75}N_{0.25}}$.

Our findings suggest that nitrogen doping of $\mathrm{LuH_3}$ can significantly alter the electronic properties of the material (bringing light elements N-$2p$ and H-$1s$ states at the Fermi level), facilitating the occurrence of superconductivity. Our results also provide insights into the band structure of the nitrogen-doped lutetium hydride, which can be used to guide the design of new superconducting materials. In particular, nitrogen doping doubles the value of DOS at the Fermi level. Simple BCS analysis shows that the critical temperature T_c for $\mathrm{LuH_{2.75}N_{0.25}}$ can exceed 100 K and one can even increase it with further hole doping by nitrogen, up to 180 K.

DATA AVAILABILITY

The raw/processed data required to reproduce these findings can be available by contacting the corresponding author. The Projected to Wannier functions Hamiltonian are available at [47].

CONFLICT OF INTEREST

The authors of this work declare that they have no conflicts of interest.

REFERENCES

1. A. P. Drozdov, M. I. Eremets, I. A. Troyan, V. Ksenofontov, and S. I. Shylin, Nature (London, U.K.) **525**, 73 (2015).
2. M. I. Eremets and A. P. Drozdov, Phys. Usp. **59**, 1154 (2016).
3. L. P. Gor'kov and V. Z. Kresin, Rev. Mod. Phys. **90**, 011001 (2018).
4. C. J. Pickard, I. Errea, and M. I. Eremets, Ann. Rev. Condens. Matter Phys. **11**, 57 (2020).
5. J. A. Flores-Livas, L. Boeri, A. Sanna, G. Profeta, R. Arita, and M. Eremets, Phys. Rep. **856**, 1 (2020).
6. I. Nekrasov and S. Ovchinnikov, J. Supercond. Novel Magn. **35**, 959 (2022).
7. I. A. Troyan, D. V. Semenok, A. G. Ivanova, A. G. Kvashnin, D. Zhou, A. V. Sadakov, O. A. Sobolevsky,

V. M. Pudalov, I. S. Lyubutin, and A. R. Oganov, Phys. Usp. **65**, 748 (2022).

8. H. Liu, I. I. Naumov, R. Hoffmann, N. W. Ashcroft, and R. J. Hemley, Proc. Natl. Acad. Sci. U. S. A. **114**, 6990 (2017).

9. I. Kruglov, R. Akashi, S. Yoshikawa, A. R. Oganov, and M. M. D. Esfahani, Phys. Rev. B **96**, 220101 (2017).

10. E. Zurek and T. Bi, J. Chem. Phys. **150**, 050901 (2019).

11. I. A. Troyan, D. V. Semenok, A. G. Kvashnin, et al., Adv. Mater. **33**, 2006832 (2021).

12. D. V. Semenok, I. A. Troyan, A. G. Ivanova, et al., Mater. Today **48**, 18 (2021).

13. N. Dasenbrock-Gammon, E. Snider, R. McBride, H. Pasan, D. Durkee, N. Khalvashi-Sutter, S. Munasinghe, S. E. Dissanayake, K. V. Lawler, A. Salamat, and R. P. Dias, Nature (London, U.K.) **615**, 244 (2023).

14. N. P. Salke, A. C. Mark, M. Ahart, and R. J. Hemley, arXiv: 2306.06301 [cond-mat].

15. K. P. Hilleke, X. Wang, D. Luo, N. Geng, B. Wang, F. Belli, and E. Zurek, Phys. Rev. B **108**, 014511 (2023).

16. Y. Sun, F. Zhang, Sh. Wu, V. Antropov, and K.-M. Ho, Phys. Rev. B **108**, L020101 (2023).

17. Z. Huo, D. Duan, T. Ma, Z. Zhang, Q. Jiang, D. An, H. Song, F. Tian, and T. Cui, Matt. Radiat. Extremes **8**, 038402 (2023).

18. M. Liu, X. Liu, J. Li, J. Liu, Y. Sun, X.-Q. Chen, and P. Liu, Phys. Rev. B **108**, L020102 (2023).

19. P. P. Ferreira, L. J. Conway, A. Cucciari, S. Di Cataldo, F. Giannessi, E. Kogler, L. T. F. Eleno, Ch. J. Pickard, Ch. Heil, and L. Boeri, Nat. Commun. **14**, 5367 (2023).

20. F. Xie, T. Lu, Z. Yu, Y. Wang, Z. Wang, Sh. Meng, and M. Liu, Chin. Phys. Lett. **40**, 057401 (2023).

21. T. Lu, Sh. Meng, and M. Liu, arXiv: 2304.06726 [cond-mat].

22. R. Lucrezi, P. P. Ferreira, M. Aichhorn, and Ch. Heil, arXiv: 2304.06685 [cond-mat].

23. A. Sufyan and J. A. Larsson, ACS Omega **8**, 9607 (2023).

24. X. Tao, A. Yang, Sh. Yang, Y. Quan, and P. Zhang, arXiv: 2304.08992 [cond-mat].

25. S.-W. Kim, L. J. Conway, Ch. J. Pickard, G. L. Pascut, and B. Monserrat, arXiv: 2304.07326 [cond-mat].

26. J. E. Hirsch, J. Supercond. Novel Magn. **36**, 1489 (2023).

27. A. Denchfield, H. Park, and R. J. Hemley, arXiv: 2305.18196 [cond-mat].

28. Đ. Dangić, P. Garcia-Goiricelaya, Y.-W. Fang, J. Ibañez-Azpiroz, and I. Errea, Phys. Rev. B **108**, 064517 (2023).

29. Sh. Zhang, J. Bi, R. Zhang, P. Li, F. Qi, Zh. Wei, and Y. Cao, AIP Adv. **13**, 065117 (2023).

30. Sh. Cai, J. Guo, H. Shu, L. Yang, P. Wang, Y. Zhou, J. Zhao, J. Han, Q. Wu, W. Yang, T. Xiang, H.-k. Mao, and L. Sun, arXiv: 2304.03100 [cond-mat].

31. N. Wang, J. Hou, Z. Liu, P. Shan, C. Chai, Sh. Jin, X. Wang, Y. Long, Y. Liu, H. Zhang, X. i Dong, and J. Cheng, arXiv: 2304.00558 [cond-mat].

32. P. Shan, N. Wang, X. Zheng, Q. Qiu, Y. Peng, and J. Cheng, Chin. Phys. Lett. **40**, 046101 (2023).

33. X. Ming, Y.-J. Zhang, X. Zhu, Q. Li, Ch. He, Y. Liu, T. Huang, G. Liu, B. Zheng, H. Yang, J. Sun, X. Xi, and H.-H. Wen, Nature (London, U. K.) **620**, 72 (2023).

34. X. Xing, Ch. Wang, L. Yu, et al., Nat. Commun. **14**, 5991 (2023).

35. Y.-J. Zhang, X. Ming, Q. Li, X. Zhu, B. Zheng, Y. Liu, Ch. He, H. Yang, and H.-H. Wen, Sci. Chin. Phys. Mech. Astron. **66**, 287411 (2023).

36. X. Zhao, P. Shan, N. Wang, Y. Li, Y. Xu, and J. Cheng, Sci. Bull. **68**, 883 (2023).

37. Zh. Liu, Y. Zhang, Sh. Huang, X. Ming, Q. Li, Ch. Pan, Y. Dai, X. Zhou, X. Zhu, H. Yan, and H.-H. Wen, arXiv: 2305.06103 [cond-mat].

38. O. Moulding, S. Gallego-Parra, P. Toulemonde, G. Garbarino, P. de Rango, S. Pairis, P. Giroux, and M.-A. Méasson, arXiv: 2304.04310 [cond-mat].

39. P. Li, J. Bi, Sh. Zhang, R. Cai, G. Su, F. Qi, R. Zhang, Zh. Wei, and Y. Cao, Chin. Phys. Lett. **40**, 087401 (2023).

40. J. Guo, Sh. Cai, D. Wang, et al., arXiv: 2306.04302 [cond-mat].

41. Zh. Li, X. He, Ch. Zhang, et al., Sci. China Phys. Mech. Astron. **66**, 267411 (2023).

42. M. Shao, S. Chen, W. Chen, K. Zhang, X. Huang, and T. Cui, Inorg. Chem. **60**, 15330 (2021).

43. G. Kresse and J. Furthmüller, Phys. Rev. B **54**, 11169 (1996).

44. J. P. Perdew, K. Burke, and M. Ernzerhof, Phys. Rev. Lett. **77**, 3865 (1996).

45. S. L. Dudarev, G. A. Botton, S. Y. Savrasov, C. J. Humphreys, and A. P. Sutton, Phys. Rev. B **57**, 1505 (1998).

46. G. Pizzi, V. Vitale, R. Arita, et al., J. Phys.: Condens. Matter **32**, 165902 (2020).

47. The projected to Wannier functions Hamiltonian for LuH$_{2.75}$N$_{0.25}$ (2023). https://github.com/PavlovNS/Lu4H11N_wannier_Hr.